59. S. Andersson and G. Bäckström, *Rev. Sci. Instrum.* **57**, 1633 (1986).
60. T. Katsura, *Phys. Earth Planet. Inter.* **101**, 73 (1997).
61. M. Osako and E. Ito, *Geophys. Res. Lett.* **18**, 239 (1991).
62. N. L. Ross and R. M. Hazen, *Phys. Chem. Miner.* **16**, 415 (1989).
63. R. Lu, A. M. Hofmeister, Y. Wang, *J. Geophys. Res.* **99**, 11795 (1994).
64. C. A. Stein and S. Stein, *Nature* **359**, 123 (1992); B. Parsons and J. G. Sclater, *J. Geophys. Res.* **82**, 803 (1977).
65. M. L. Renkin and J. G. Sclater, *ibid.* **93**, 2919 (1988); J. G. Sclater and L. Wilson, in *The Geology of North America: The Western North Atlantic,* P. R. Vogt and B. E. Tucholke, Eds. (Geological Society of America, Boulder, CO, 1986), pp. 257–270.
66. This approach is consistent with solutions of steady-state heat flow between stacked parallel planes [see section 3.2 in (*1*)]. It is reasonable because the pressure dependence is weak (κ doubles over 760 km).
67. A. M. Dziewonski and D. L. Anderson, *Phys. Earth Planet. Inter.* **25**, 297 (1981).
68. T. Inoue and H. Sawamoto, in (*7*), pp. 323–331. The 1-atm value is the same as the dry solidus [see A. E. Ringwood, *Composition and Petrology of the Earth's Mantle* (McGraw-Hill, New York, 1975)].
69. J. B. Gaherty, T. H. Jordon, L. S. Gee, *J. Geophys. Res.* **101**, 22291 (1996).
70. Y. Xu and D. A. Weins, *ibid.* **102**, 27439 (1997).
71. E. Takahashi, *ibid.* **91**, 9367 (1986).
72. D. L. Turcotte and G. Schubert, *Geodynamics* (Wiley, New York, 1982).
73. E. Ito and T. Katsura, *Geophys. Res. Lett.* **16**, 425 (1989).
74. E. Ito and E. Takahashi, *J. Geophys. Res.* **94**, 10637 (1989); E. Ito and T. Katsura, in (*7*), pp. 315–322.
75. D. C. Presnall, Y. H. Weng, C. S. Milholland, M. J. Walter, *Phys. Earth Planet. Inter.* **107**, 83 (1998).
76. E. Ohtani, K. Moriwaki, T. Kato, K. Omuma, *ibid.,* p. 75.
77. A. Zerr, A. Diegeler, R. Boehler, *Science* **281**, 243 (1998).
78. T. Katsura and E. Ito, *J. Geophys. Res.* **94**, 15663 (1986).
79. F. D. Stacey, *Phys. Earth Planet. Inter.* **15**, 341 (1977).
80. J. M. Brown and T. J. Shankland, *Geophys. J. R. Astron. Soc.* **66**, 579 (1981).
81. R. Boehler, *Earth Planet. Sci. Lett.* **111**, 217 (1992).
82. _____, *Annu. Rev. Earth Planet. Sci.* **24**, 15 (1996); F. D. Stacey, in preparation.
83. F. D. Stacey and D. E. Loper, *Phys. Earth Planet. Inter.* **33**, 45 (1983).
84. D. L. Anderson, *Theory of the Earth* (Blackwell Scientific, Boston, 1989).
85. J. Verhoogen, *Phys. Earth Planet. Inter.* **7**, 47 (1973); F. D. Stacey, *Physics of the Earth* (Brookfield, Brisbane, Australia, 1992).
86. O. L. Anderson, *Phys. Earth Planet. Inter.* **109**, 179 (1998).
87. S. Zhong and M. Gurnis, *J. Geophys. Res.* **99**, 15683 (1994); B. H. Hager, *Eos* **71**, 1567 (1990).
88. Y. Sumino and O. Anderson, in *Handbook of Physical Properties of Rocks III*, R. S. Carmichael, Ed. (CRC Press, Boca Raton, FL, 1984), pp. 139–280; J. D. Bass, in (*50*), pp. 45–63; E. Knittle, *ibid.,* pp. 98–142.
89. H. Cynn and A. M. Hofmeister, *J. Geophys. Res.* **99**, 17717 (1994).
90. T. Ashida, S. Kume, E. Ito, A. Navrotsky, *Phys. Chem. Miner.* **16**, 239 (1988).
91. A. M. Hofmeister, in (*34*), pp. 215–227.
92. A. E. Beck, D. M. Darba, H. H. Schloessin, *Phys. Earth Planet. Inter.* **17**, 35 (1978).
93. G. H. Scharmli, in *High Pressure Research in Geosciences*, W. Schreyer, Ed. (Schweizerbartsche, Stuttgart, Germany 1982), pp. 349–373.
94. H. H. Schloessin and Z. Dvorak, *Geophys. J. R. Astron. Soc.* **27**, 499 (1972).
95. M. Osako and Y. Kobayashi, *Phys. Earth Planet. Inter.* **18**, P1 (1979).
96. S. W. Kieffer, I. C. Getting, G. C. Kennedy, *J. Geophys. Res.* **81**, 3018 (1976).
97. K. Horai and J. Sasaki, *Phys. Earth Planet. Inter.* **55**, 292 (1989).
98. Å. Franson and R. G. Ross, *J. Phys. C Solid State Phys.* **12**, 219 (1983).

99. I thank R. Boehler for suggesting this problem, the Humboldt Foundation for making our interaction possible, and the David and Lucile Packard Foundation for funding the IR spectroscopy that formed the basis of this study. The input of O. L. Anderson, A. Chopelas, R. E. Criss, R. F. Dymek, S. A. Hauck, R. Phillips, P. Shore, M. Simons, D. Weins, M. Wyssession, and four anonymous reviewers is greatly appreciated. The project was partially supported by NSF grant EAR712311.

25 August 1998; accepted 4 January 1999

A Well-Collimated Quasi-Continuous Atom Laser

E. W. Hagley,[1] L. Deng,[1,2] M. Kozuma,[3] J. Wen,[1] K. Helmerson,[1] S. L. Rolston,[1] W. D. Phillips[1]

Extraction of sodium atoms from a trapped Bose-Einstein condensate (BEC) by a coherent, stimulated Raman process is demonstrated. Optical Raman pulses drive transitions between trapped and untrapped magnetic sublevels, giving the output-coupled BEC fraction a well-defined momentum. The pulsed output coupling can be run at such a rate that the extracted atomic wave packets strongly overlap, forming a highly directional, quasi-continuous matter wave.

The occupation of a single quantum state by a large number of identical bosons (*1–5*) is a matter-wave analog to the storage of photons in a single mode of a laser cavity. Just as one extracts a coherent, directed beam of photons from a laser cavity by using a partially transmitting mirror as an output coupler, one can analogously extract directed matter waves from a condensate. Such a source of matter waves, or "atom laser," is important in the field of atom optics (*6*), the manipulation of atoms analogous to the manipulation of light. Its development is providing atom sources that are as different from ordinary atomic beams as lasers are from light bulbs.

The first demonstration of a BEC output coupler was reported in 1997 (*7*) where coherent, radiofrequency (rf)-induced transitions were used to change the internal state (magnetic sublevel) of the atoms from a trapped to an untrapped state. This method, however, did not allow the direction of the output-coupled atoms to be chosen. The extracted atoms fell under the influence of gravity and expanded because of their intrinsic repulsion. We demonstrate a highly directional method to optically couple out a variable fraction of a condensate and apply this method to produce a well-collimated, quasi-continuous beam of atoms, an important step toward a truly continuous wave (cw) atom laser (*8*).

The output coupling is based on stimulated Raman transitions between magnetic sublevels (*9, 10*). The sublevel into which the atoms are transferred is unaffected by the trapping potential, and the process imparts a well-defined momentum to the output-coupled condensate fraction. In contrast, previous work on Bragg diffraction (*11*) transferred momentum without changing the internal state of the atom. A single Raman pulse can couple out any desired fraction of the condensate. By changing the angle between the wave vectors $\boldsymbol{k}$ of the Raman lasers ($k = 2\pi/\lambda$, $\lambda = 589$ nm) and using higher order ($2n$-photon) Raman transitions, it is possible to impart any momentum of magnitude 0 to $2n\hbar k$ (*11*) to the atoms (for sodium, $2\hbar k$ corresponds to a velocity of 6 cm/s). In this way it is possible to choose the energy of the extracted deBroglie wave, producing a widely tunable atom laser.

In this experiment, we used a hybrid evaporation technique with a time orbiting potential (TOP) trap (*12, 13*) to form a sodium condensate (*11*). We typically obtain a condensate, without a discernible normal fraction, with about 10^6 atoms in the $3S_{1/2}$, $F = 1$, $m = -1$ state (*14*). Once the condensate is formed we adiabatically expand the trapping potential in 0.5 s, reducing the trapping frequencies to $\omega_x/2\pi = 18$ Hz, $\omega_y/2\pi = 25$ Hz, and $\omega_z/2\pi = 35$ Hz. We have measured (*15*) that our adiabatic cooling reduces the asymptotic root mean square (rms) momentum width of the released condensate to $0.09(1)\hbar k$ (*16*).

In Raman output coupling (Fig. 1), a moving standing wave, composed of two nearly counterpropagating laser beams with frequency difference $\delta = \omega_2 - \omega_1$ (*17*), is

[1]National Institute of Standards and Technology, Gaithersburg, MD 20899, USA. [2]Georgia Southern University, Statesboro, GA 30460, USA. [3]Institute of Physics, University of Tokyo, Tokyo 153-8902, Japan.

applied to the condensate for a short period of time. These beams propagate nearly along the $\hat{z}$ axis of the trap (gravity is along $\hat{x}$) and each beam is detuned from the $3S_{1/2}$, $F = 1 \rightarrow 3P_{3/2}$, $F' = 2$ transition by $\Delta/2\pi = -1.85$ GHz to suppress spontaneous emission. A stimulated Raman transition occurs when an atom changes its state by coherently exchanging photons between the two laser beams (absorption from ω_1 and stimulated emission into ω_2). The atom acquires momentum $\boldsymbol{P} = \hbar(\boldsymbol{k}_1 - \boldsymbol{k}_2) = P\hat{z}$ (in our case) with $P = 2\hbar k \sin(\theta/2)$ (*18*). Therefore, an atom initially at rest acquires kinetic energy $\hbar\delta_{\mathrm{Recoil}} = P^2/(2M)$, where M is the atomic mass. The stimulated Raman process can change the internal energy state of an atom by driving $\Delta m = 1$ or even $\Delta m = 2$ transitions (*19*). The energy difference between the absorbed and emitted photons must account for both the change in kinetic energy and any change in the internal (magnetic) energy level of the atom: $\hbar\delta = \hbar\delta_{\mathrm{Zeeman}} - \hbar\delta_{\mathrm{recoil}}$. By changing the internal state of a trapped atom to $m = 0$, a state that feels no trapping forces, we release the atoms and impart a momentum that kicks them away.

Our Raman output coupling scheme dramatically reduces the transverse momentum width of the extracted atoms compared with other methods such as rf output coupling (*7*). The $0.09(1)\hbar k$ rms momentum width discussed previously corresponds to the average release energy of $2/7\mu$ (the chemical potential $\mu \propto N^{2/5}$, where N is the number of atoms in the condensate) per atom caused by the intrinsic repulsion between the atoms. If, however, only a small number of atoms are coupled out of the condensate into the $m = 0$ state, the average energy per extracted atom is two times larger (*20*). For atoms coupled out of a spherically symmetric trap without an initial momentum kick, this release energy causes an isotropic momentum spread. In our case, where significant momentum is imparted to the atoms, the release energy is primarily channeled into the forward direction. This dramatically reduces the transverse rms momentum width, resulting in a highly collimated output beam. The transverse momentum width (*21*) is reduced by roughly the ratio of the characteristic time it takes the output-coupled atoms to leave the still-trapped condensate divided by the time scale over which the mean field repulsion acts on the freely expanding condensate (*22*) and will therefore be extremely small compared with its longitudinal momentum of $2\hbar k$. This has been confirmed by numerical calculations, which estimate the mean field component of the transverse rms momentum width to be $0.004\hbar k$.

The uncertainty principle imposes an additional transverse momentum width of $0.002\hbar k$ due to the finite size of the condensate. The predicted mean-field momentum width is close to this lower limit and corresponds to a divergence of a few milliradians, comparable to that of a typical commercial optical laser. As this momentum width is so small, it is difficult to measure experimentally (during the typical 7-ms duration of the experiment the radius of the atomic cloud would expand only 1 μm).

To implement this Raman output coupling scheme requires that special attention be paid to the time-varying magnetic field in a TOP trap. In the presence of gravity the atoms sag (in this case about 0.8 mm) away from the center of the trap to a position where the magnitude of the magnetic field changes as the bias field rotates (*23*). The time-dependent detuning for the two-photon transition is

$$\delta(t) = \frac{\Delta m \mu_B}{2\hbar} |\mathbf{B}(t)| - \frac{2\hbar k^2 \sin^2(\theta/2)}{M} \quad (1)$$

where μ_B is the Bohr magneton and $\Delta m = 0$, 1, or 2. The frequency difference between $m = -1$ and $m = 0$ sublevels changes by nearly 4 MHz as the TOP field rotates. This frequency difference is large compared with the effective width of the transition, the inverse of the Raman pulse length (typically 6 μs). Therefore, the Raman pulse is synchronized to the maximum value of $\delta(t)$ to minimize variations in the resonance frequency during the transition. Compared with continuous output coupling, this pulsed Raman output coupling results in less spontaneous emission for the same percentage of output-coupled atoms.

When the Raman pulses were applied, the magnetic field direction was along the $\hat{x}$ axis (vertical), as was the polarization of one of the two Raman lasers [which drove only $\Delta m = 0$ (π) transitions]. This laser had an intensity of 300 mW/cm^2 (*24*). The second Raman laser drove $\Delta m = 1$ (σ) transitions when its polarization was along $\hat{y}$ and it had an intensity of 600 mW/cm^2, but only half this power was useful because of selection rules. For $\Delta/2\pi = -1.85$ GHz, this intensity corresponds to an average time per atom between spontaneous emission events of 70 μs.

Directional output coupling is observed by imaging the atoms several milliseconds after the Raman pulse. Figure 2 shows optical depth images obtained by first optically pumping the atoms to the $3S_{1/2}$, $F = 2$ state and then absorption-imaging (*2*) on the $3S_{1/2}$, $F = 2 \rightarrow 3P_{3/2}$, $F' = 3$ transition. The sequence (Fig. 2, A to C) shows a BEC ($F =$

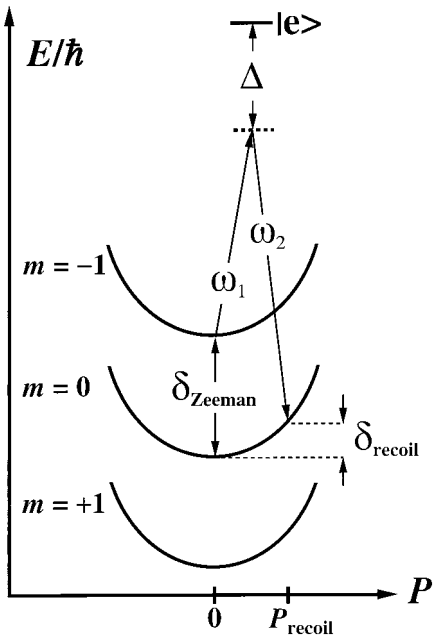

Fig. 1. Principle of the Raman output coupler. Energy conservation requires a relative detuning, $\delta = \omega_2 - \omega_1$, between the Raman lasers. Total energy as a function of atomic momentum is plotted, where the parabolas correspond to kinetic energy $P^2/2M$.

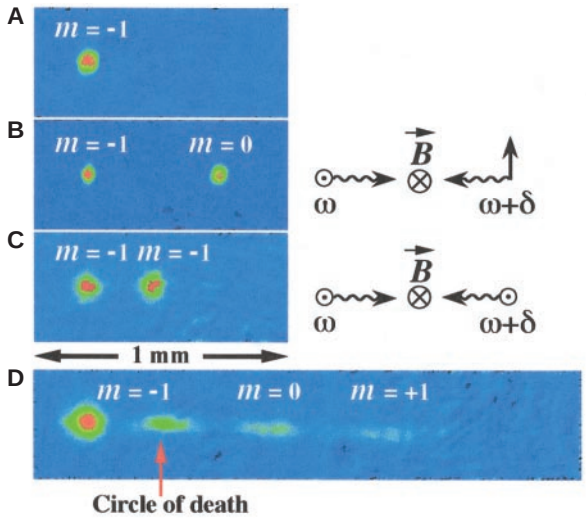

Fig. 2. (**A**) Condensate before the application of a Raman pulse. (**B**) $\Delta m = +1$ transition (*19*) from a 6-μs pulse with $\delta/2\pi = 6.4$ MHz. This detuning is chosen to be slightly larger than the 6.27-MHz resonance frequency to suppress four-photon coupling to the $m = +1$, $4\hbar k\hat{z}$ state (*25*). (**C**) $\Delta m = 0$ transition (*26*) after a 14-μs Raman pulse with equal laser intensities of 25 mW/cm^2. The relative detuning was $\delta/2\pi = -98$ kHz and the polarizations of both lasers were aligned with $\hat{x}$. The diagrams to the right of (B) and (C) show the polarization of the lasers with respect to the local magnetic field. We verified that no transitions occurred when incorrect polarizations were used. (**D**) The rotating magnetic field zero (circle of death) results in Majorana transitions of an output-coupled condensate fraction in the $m = 0$ state. Arrow denotes physical location of the rotating bias field zero. This is a graphic depiction of Majorana transitions.

1, $m = -1$) followed by two BECs after application of a single Raman pulse. The TOP trap confining fields were held on for 7 ms after application of the Raman pulse before being switched off. The system was then allowed to evolve freely for 1.6 ms before being imaged. Note that the position of the output-coupled atoms in Fig. 2B is different from that in Fig. 2C. In the former, the atoms that have undergone the Raman transition are in the state $m = 0$ and therefore no longer feel the trapping potential, whereas in Fig. 2C the atoms are still trapped. The position of the $m = 0$ atoms corresponds to free flight with momentum $2\hbar k\hat{z}$ during the entire 8.6 ms, whereas the position of the atoms in Fig. 2C corresponds to their classical turning point in the trap (7 ms is about one-quarter of the 28.6-ms oscillation period along $\hat{z}$).

In the case where the detuning of the lasers from the excited state is large compared with the excited-state hyperfine structure splitting, it is not possible to drive $\Delta m = 2$ transitions directly with two photons because the ground state looks like a spin 1/2 system for which there are only two states. Instead, we can couple to the $m = +1$ state by combining the Raman process with Majorana transitions due to the TOP rotating magnetic field zero (*13*). Atoms were first output-coupled to the $m = 0$ state and imaged 10.6 ms later after having crossed the orbit of the zero of the magnetic field (*27*), known as the "circle of death," which orbits in the $\hat{x}$-$\hat{z}$ plane (Fig. 2D). For this image the rotating bias field was reduced by a factor of 3, which reduced the distance to the orbiting magnetic field zero to 0.3 mm. As the atoms crossed this orbit they lost their quantization axis and were repeatedly projected to all three magnetic sublevels at the 20-kHz TOP frequency. The atoms in $m = -1$, 0, and $+1$ states were, respectively, retarded, unimpeded, and ejected by the trapping potential, giving rise to three spatially separated stripes of atoms. At the time of imaging, the atoms that ended in the $m = -1$ state have already been pulled back to the circle of death by the trap.

Although it is not possible to drive the $\Delta m = 2$ transition with two photons, it is possible with four by using the $m = -1 \rightarrow m = 0 \rightarrow m = +1$ transition scheme (Fig. 3C). A single 6-μs Raman pulse with $\delta/2\pi = 6.15$ MHz and the same intensities used for Fig. 2B was applied. In Fig. 3A, the TOP was switched off immediately after the Raman pulse and the atoms were imaged 5.6 ms later. The $m = +1$ atoms received $4\hbar k\hat{z}$ of momentum from four photons, and the $m = 0$ atoms received only $2\hbar k\hat{z}$ from two photons; thus the $m = +1$ atoms moved twice as far as the $m = 0$ atoms. With the TOP switched off 4 ms after the Raman pulse and the system imaged 1.6 ms later (Fig. 3B), the atoms in the $m = +1$ antitrapped state are accelerated away from the trap, causing them to move further.

To produce quasi-continuous output coupling, we used multiple Raman pulses. The laser intensities were reduced and the detuning was again chosen to be $\delta/2\pi = 6.4$ MHz to primarily couple to the $m = 0$ state. For the optical depth images of the condensate after one, three, and six Raman pulses (Fig. 4, A to C), the TOP was held on for a 9-ms window during which time 6-μs Raman pulses were fired at a subharmonic of the rotating bias frequency. The magnetic fields were then extinguished and the atoms were imaged 1.6 ms later. The intensity of the laser whose polarization was aligned with $\hat{x}$ was 300, 150, and 100 mW/cm^2, respectively, to couple out different fractions of the condensate (the intensity of the second Raman laser was twice that of the first).

In Fig. 4D the TOP trap was held on during a 7-ms window during which time 140 Raman pulses were fired at the 20-kHz frequency of the rotating bias field and the distribution of atoms was imaged 1.6 ms later. The Raman pulse duration and intensity were reduced to 1 μs and 40 mW/cm^2 for Fig. 4D to ensure that the total integrated pulse time of 140 μs was much less than the spontaneous emission time of about 500 μs. The phase of the output-coupled matter wave evolves at about 100 kHz with respect to the condensate itself because of the kinetic energy imparted by the two-photon Raman transition (*28*). Because 100 kHz is an integer multiple of the ~20-kHz output coupling repetition rate, the interference of successive pulses is almost completely constructive (*29*). In the time between two Raman pulses each output-coupled wave packet moves only 2.9 μm, much less than the ~50-μm size of the condensate, so the output-coupled atoms form a quasi-continuous coherent matter wave. By varying the delay between pulses, the interference between wave packets can be used to investigate the coherence properties of the condensate.

It is apparent that there is also coupling to the $m = +1$ state in Fig. 4D because some output-coupled atoms have moved the distance that an atom with momentum $4\hbar k\hat{z}$ moves in 8.6 ms. Such coupling to the $m = +1$ state occurs in this case because the spectral width of the 1-μs Raman pulse is sufficiently broad (*30*) to drive a transition from the state $m = 0$ (momentum $2\hbar k\hat{z}$) to the state $m = +1$ (momentum $4\hbar k\hat{z}$). In our experiment the trajectories of the two output-coupled beams ($m = 0$ and $m = +1$) are spatially separated because the direction of momentum transfer is orthogonal to gravity. These two beams appear to overlap in Fig. 4D because the camera views them from above. Coupling to the $m = +1$ state could be suppressed by using a larger bias magnetic field and a larger detuning Δ to exploit the second-order Zeeman shift and to reduce the pulse bandwidth without excessive spontaneous emission. To completely suppress

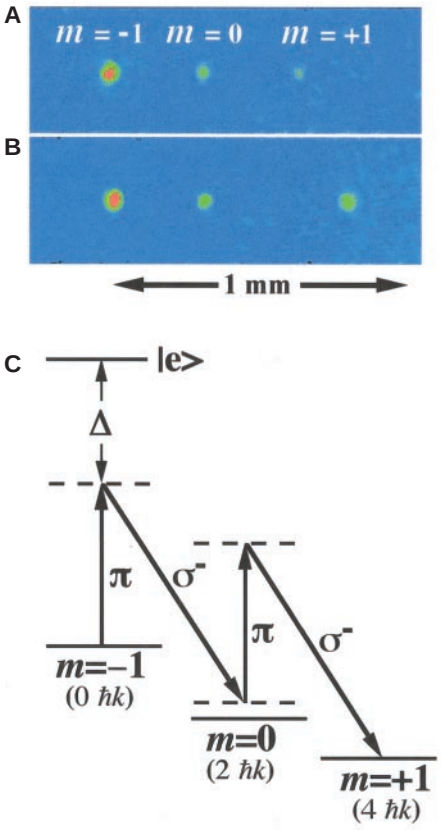

Fig. 3. Atoms are coupled to both the $m = 0$ and $m = +1$ and magnetic sublevels using a single Raman pulse. (**A**) Magnetic trap is switched off immediately after the Raman pulse. (**B**) Magnetic trap is held on for 4 ms after the Raman pulse. (**C**) Transition used and laser polarizations.

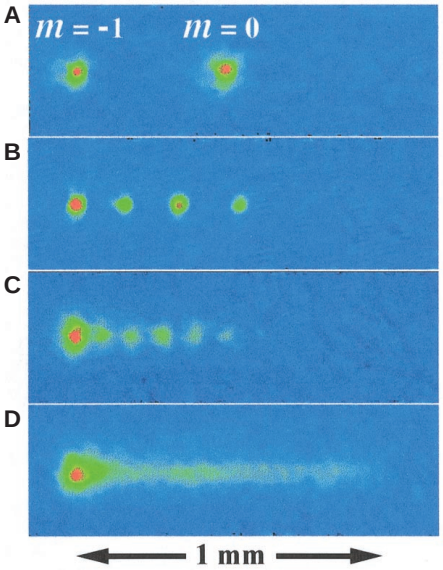

Fig. 4. (**A** to **C**) One, three, and six 6-μs Raman pulses, respectively, were applied to the condensate. (**D**) Firing 1-μs Raman pulses at the full repetition rate of about 20 kHz imposed by the frequency of the rotating bias field (140 pulses in 7 ms) produces a quasi-continuous atomic beam.

coupling to unwanted antitrapped states a Raman transition to the $F = 2, m = 0$ ground state of Na could be used.

An important property of the condensate, and any output-coupled fraction, is its coherence. Coherence effects between two condensates have already been observed by dropping them and allowing them to interfere (*30*). Because we use a stimulated Raman process, our output beam should be fully coherent. The effect of the mean field on the atoms as they leave the BEC will be to distort the outgoing wave without resulting in any true loss of coherence. In a separate experiment we observed matter-wave interference due to the 100-kHz phase evolution discussed above and we are using it to measure the coherence properties of the condensate.

References and Notes

1. A. Einstein, *Sitzungsbe. Kgl. Preuss. Akad. Wiss.* (1924), p. 261; *ibid.* (1925), p. 3.
2. M. H. Anderson, J. R. Ensher, M. R. Matthews, C. E. Wieman, E. A. Cornell, *Science* **269**, 198 (1995).
3. K. B. Davis *et al., Phys. Rev. Lett.* **75**, 3969 (1995).
4. C. C. Bradley, C. A. Sackett, R. G. Hulet, *ibid.* **78**, 985 (1997); see also C. C. Bradley, C. A. Sackett, J. J. Tollett, R. G. Hulet, *ibid.* **75**, 1687 (1995).
5. D. G. Fried *et al., ibid.* **81**, 3807 (1998).
6. *J. Physique* **4**, 11 (1994); *Appl. Phys. B.* **54**, 321 (1992); *J. Phys. Rep*. 240 (1994) (special issues on optics and interferometry with atoms).
7. M.-O. Mewes *et al., Phys. Rev. Lett.* **78**, 582 (1997).
8. A truly cw atom laser produces a continuous, coherent matter wave output while being continuously replenished with new atoms, in direct analogy with a cw optical laser. The coherence length of such a laser would be longer than the size of the trapped condensate just as the coherence length of a cw optical laser is longer than the laser cavity.
9. G. Moy, J. Hope, C. Savage, *Phys. Rev. A* **55**, 3631 (1997).
10. M. A. Edwards, C. W. Clark, K. Burnett, S. L. Rolston, W. D. Phillips, *J. Phys. B*, in press.
11. M. Kozuma *et al., Phys. Rev. Lett.* **82**, 871 (1999).
12. Our TOP trap is different from previous TOP traps (*13*) because the rotating bias field orbits in a plane that includes the quadrupole axis. The field gradient along the quadrupole axis ($\hat{z}$) is 9.2 T/m, and the rotating bias field is 1.0 mT. The time-averaged magnetic field forms a trap with harmonic frequencies $\omega_x/2\pi = 180$ Hz, $\omega_y/2\pi = 250$ Hz, and $\omega_z/2\pi = 360$ Hz.
13. W. Petrich, M. H. Anderson, J. R. Ensher, E. A. Cornell, *Phys. Rev. Lett.* **74**, 3352 (1995).
14. Atoms in the state $m = -1$ are trapped by the magnetic fields, whereas those in state $m = +1$ are antitrapped. The state $m = 0$ does not feel the confining potential of the magnetic trap.
15. This was done by switching off the trap and measuring the rate of the mean-field-driven ballistic expansion of the condensate at long times (>10 ms).
16. All uncertainties reported in this paper are 1-SD combined statistical and systematic uncertainties.
17. For frequency stability, both beams are derived from a single dye laser with the frequency difference controlled by two acousto-optical modulators.
18. θ, which equals 166° in this case, is the angle between $\boldsymbol{k}_1$ and $\boldsymbol{k}_2$, and $|\boldsymbol{k}_1| \approx |\boldsymbol{k}_2| = k$. Therefore, $P = 1.99\hbar k \approx 2\hbar k$.
19. We define $\Delta m = m_{\text{final}} - m_{\text{initial}}$. $m_{\text{initial}} = -1$ is the only magnetically trapped state.
20. Assuming that the scattering lengths among all m states are the same, this can be derived from expressions found in [F. Dalfovo, S. Giorgini, L. P. Pitaevskii, S. Stringari, *Rev. Mod. Phys.* **71**, 2 (1999)]. The energy needed to add one atom is μ, which has a magnetic contribution of 3/7 μ and a mean-field contribution of 4/7 μ. If a small number of atoms are ouput-coupled to $m = 0$, a state that is not magnetically trapped, their release energy will simply be 4/7 μ, or twice the average release energy of 2/7 μ for the whole condensate.
21. In addition, the longitudinal momentum width is reduced by about the same factor because of kinematic compression.
22. The characteristic time during which the mean field potential energy turns into kinetic energy in the released BEC is $1/\bar{\omega}$ (in our case about 6 ms), where $\bar{\omega}$ is the geometric mean of the three trapping frequencies. For our two-photon Raman transition the characteristic time scale for leaving the region of the condensate is 300 μs.
23. This is because our TOP field rotates in $\hat{x}$-$\hat{z}$ plane, which includes the direction of gravity.
24. The power quoted was the average over a 3-mm-diameter aperture in the center of a somewhat inhomogeneous 7-mm beam. These powers were empirically chosen to produce good output coupling.
25. The resonance frequency, for the $\Delta m = 2$ four-photon transition discussed later, was found to be 6.15(5) MHz, in good agreement with the calculated value of 6.0(2) MHz based on measurements of the trapping magnetic fields. This additional detuning of 2×250 kHz = 500 kHz from the four-photon resonance frequency is large compared with the Fourier width of the Raman pulse and results in a suppression of coupling to the $4\hbar k\hat{z}$, $m = +1$ state.
26. A stimulated Raman transition that changes the momentum state of an atom but does not change the internal energy state can be viewed as Bragg diffraction (*11*); see also P. J. Martin, B. G. Oldaker, A. H. Miklich, D. E. Pritchard, *Phys. Rev. Lett.* **60**, 515 (1988).
27. Because of our choice of applying the Raman beams along the quadrupole axis of the trap ($\hat{z}$), the trajectory of the output-coupled atoms (initially along $\hat{z}$) lies in the $\hat{x}$-$\hat{z}$ plane because gravity is along $\hat{x}$. This is the plane of the rotating magnetic field zero and so the atoms will, at some point in time, cross this circle of death.
28. In the case of $\theta = 180°$ the recoil momentum from a first-order Raman transition is exactly $2\hbar k\hat{z}$, which corresponds to a frequency of 100.1 kHz.
29. This was confirmed in a separate experiment, which looked at the interference of two clouds of atoms diffracted out of the condensate.
30. If the output coupling process were made continuous, by using an optical dipole or magnetic trap with no time-dependent magnetic fields, such coupling would not occur because the Fourier width of the light pulse could be made arbitrarily small. It would therefore be a simple matter to make a continuous Raman output coupler in such a case.
31. M. R. Andrews *et al., Science* **273**, 637 (1997).

32. Supported in part by the Office of Naval Research and NASA. M.K. acknowledges the support of the Japanese Society for the Promotion of Science for Young Scientists. We thank C. W. Clark, M. A. Edwards, and P. S. Julienne for their valuable comments and suggestions.

24 November 1998; accepted 3 February 1999

Quantum-Well States as Fabry-Pérot Modes in a Thin-Film Electron Interferometer

J. J. Paggel, T. Miller, T.-C. Chiang*

Angle-resolved photoemission from atomically uniform silver films on iron (100) shows quantum-well states for absolutely determined film thicknesses ranging from 1 to ~100 monolayers. These states can be understood in terms of Fabry-Pérot modes in an electron interferometer. A quantitative line shape analysis over the entire two orders of magnitude of thickness range yields an accurate measurement of the band structure, quasiparticle lifetime, electron reflectivity, and phase shift. Effects of confinement energy gap, reflection loss, and surface scattering caused by controlled roughness are demonstrated.

Quantum mechanics is based on wave-particle duality, which is well documented through diffraction and interference experiments using particles (*1*). Thus, there is a close analogy between a standing electromagnetic wave between two reflecting surfaces and an electron confined in a square potential well (*2*). The former case corresponds to the Fabry-Pérot interferometer (*3*), which shows a set of peaks in optical transmission. The latter case, an electron quantum well, can be realized in a thin solid film. Electron confinement within a film results in discrete quantum-well states observable by angle-resolved photoemission (*4*). Photoemission, however, involves an optical transition. This can lead to complications, and the line shape is generally quite complex even for simple systems (*5, 6*). Nevertheless, we show here that photoemission spectra of quantum-well states can be analyzed in the same way as an optical Fabry-Pérot interferometer filled with a medium. The dispersive and absorptive properties of this medium account for the electronic band structure and quasiparticle lifetime.

The Ag on Fe(100) system was chosen for this study because of its rather unique property that atomically uniform films can be prepared for thicknesses ranging from 1 to ~100 monolayers (ML) (*7*). Layer counting leads to an absolute determination of thickness, and a sin-

Department of Physics, University of Illinois, 1110 West Green Street, Urbana, IL 61801, USA, and Frederick Seitz Materials Research Laboratory, University of Illinois, 104 South Goodwin Avenue, Urbana, IL 61801, USA.

*To whom correspondence should be addressed. E-mail: t-chiang@uiuc.edu